Additive-enhanced hydrogen- and hydroxide-based magneto-ionic control in Ni films

M. Kutuzau,[1,2,3] M. Gößler,[1,4] S. Topolovec,[4] S. Schiemenz,[2] D. Wolf,[2] M. Richter,[2,5] K. Nielsch,[2,6] and K. Leistner[1,2]

[1]*Electrochemical Sensors and Energy Storage, Institute of Chemistry, Faculty of Natural Sciences, Chemnitz University of Technology, Strasse der Nationen 62, 09111 Chemnitz, Germany*

[2]*Leibniz IFW Dresden, Helmholtzstrasse 20, 01069 Dresden, Germany*

[3]*Sustainable Technologies for Industrial Processes (STIP), Netherlands Organization for Applied Scientific Research (TNO), Westerduinweg 3, 1755LE Petten, Netherlands*

[4]*Institute of Materials Physics, Graz University of Technology, NAWI Graz, Petersgasse 16, 8010 Graz, Austria*

[5]*Dresden Center for Computational Materials Science (DCMS), TU Dresden, 01062 Dresden, Germany*

[6]*Institute of Material Science, TU Dresden, 01062 Dresden, Germany*

(Received 25 July 2025; accepted 20 October 2025; published 12 November 2025)

Magneto-ionic control of metals is a promising approach for energy-efficient and voltage-programmable magnetic devices. In this work, we demonstrate a dual hydrogen- and hydroxide-ion-based mechanism to control the magnetic properties of nickel films in an alkaline electrolyte. Upon application of reduction potentials, reversible electrochemical hydrogen absorption into a nickel film electrode is found to decrease its overall magnetic moment, while an increase in the overall magnetic moment at more negative potentials can be explained by the reduction of nickel hydroxide on the surface. Furthermore, coercivity is also decreased in the reduced state. This effect is reversible over 50 reduction-oxidation cycles and reaches up to 30% change at maximum. The addition of thiourea to the electrolyte amplifies the magnitude of the magneto-ionic control of the magnetic moment by a factor of 2 and promotes the energy efficiency of the magneto-ionic effect by decreasing the required overpotentials by ∼0.25 V. *In situ* Raman spectroscopy reveals the formation of an α-$Ni(OH)_2$ layer on the Ni surface in the presence of thiourea, which may be the cause for the improved magneto-ionic effect. Our study not only introduces Ni as a versatile magneto-ionic material, but also demonstrates how electrolyte additives can be used to boost magneto-ionic effects in terms of effect strength and energy efficiency.

DOI: 10.1103/29bv-d9j4

I. INTRODUCTION

Magneto-ionic mechanisms rely on voltage-triggered ionic motion and redox-reactions to tune magnetic properties with excellent energy efficiency [1–4]. Voltage-controlled low-power, magneto-ionic systems can be a contribution toward a greener future by replacing electric-current-controlled magnetic devices. To date, micro-electromagnets are embedded in hard disc drive heads, and high spin polarized currents ($10^9 - 10^{12}$ A/m^2) are used to switch magnetization in spin transfer torque magnetic random access memories and domain wall logic devices [5,6]. The energy consumption as a result of the Joule heating associated with the electric current flow in such devices is a major disadvantage [7]. Magneto-ionic materials, in contrast, are controlled by an electric voltage and require only a negligible electric current for setting the magnetic state. In addition, magneto-ionic mechanisms can work at room temperature and low voltage (∼1 V) [3]. This is an advantage over most other magneto-electric material systems for voltage control of magnetism, which are usually restricted to low temperatures and/or require high voltages (∼kV) [3,8,9]. Thus, magneto-ionic control currently presents a thriving approach to reduce energy consumption by the development of ultralow power sensors, actuators, data storage and computing devices [4,8,10–12].

The main principle of magneto-ionic control is that an external voltage is applied to a magnetic material via a solid or liquid electrolyte [3]. The voltage induces reversible ionic motion and oxidation/reduction reactions, which in consequence impact the magnetic properties. This way, voltage-tunable magnetism has been demonstrated in a multitude of oxides, metals, and alloys [13–19]. Especially the sensitivity of the ferromagnetic *3d* metals to magneto-ionic control is promising in view of potential applications, as their high magnetization can be exploited at room temperature.

Magneto-ionic effects in ferromagnetic metals are usually investigated with regard to one specific ionic species, such as oxygen, hydroxide, lithium, nitrogen, or hydrogen ions [3,4]. So far, the most-studied magneto-ionic systems involve oxygen/hydroxide [16,20–25] and hydrogen [18,26,27] ions. Oxygen/hydroxide-based magneto-ionic effects typically rely on metal oxide or metal hydroxide reduction and subsequent metal re-oxidation processes. Hence, a change of the phase and the related magnetic state (e.g.,

Published by the American Physical Society under the terms of the Creative Commons Attribution 4.0 International license. Further distribution of this work must maintain attribution to the author(s) and the published article's title, journal citation, and DOI.

paramagnetic iron oxide versus ferromagnetic iron metal) occurs, and the observed effects are drastic. Examples are the voltage-controlled ON/OFF switching of (i) magnetism [24,28] and (ii) coercivity [29] caused by the change in (i) magnetization and (ii) pinning strength, when the metal-oxide transformation takes place. Because of the limited diffusion ability of oxygen and hydroxide ions in metals, the redox reactions causing the magneto-ionic effects are typically restricted to interface regions up to a thickness of a few nanometers [22,30]. In consequence, the oxygen/hydroxide-based magneto-ionic effects are largest for ultrathin films [20,29,31], nanoislands [17], or nanoporous structures [32], where the interface contribution is large and thus the effects are pronounced. In contrast, the hydrogen-based magneto-ionic control relies on the voltage-triggered electrochemical reduction of water molecules or protons to adsorbed hydrogen atoms (H_{ads}) [see reaction Eqs. (1) and (2)], which can be absorbed in the material (H_{abs}), [see reaction Eq. (3)],

$$H^+ + e^- \rightarrow H_{ads}(\text{in acidic media}), \tag{1}$$

$$H_2O + e^- \rightarrow H_{ads} + OH^-(\text{in alkaline media}), \tag{2}$$

$$H_{ads} \rightarrow H_{abs}. \tag{3}$$

The magnetic properties of the material acting as a working electrode can then be controlled via hydrogen adsorption and/or absorption. Hydrogen adsorption influences interfacial magnetic properties, such as magnetic interface anisotropy in Co films [26,33]. In contrast, hydrogen absorption proceeds via hydrogen diffusion into the material volume and thus affects volumetric magnetic properties, which recently opened up the possibility to voltage control the coercivity of micron-scale $SmCo_5$ [18] and Co/Pd multilayers [34,35] or magnetization in nanoporous PdCo [36]. For thin films, the hydrogen-based mechanism offers fast switching times in the range of milliseconds [26].

The combination of different ionic species in magneto-ionics seems exciting with regard to an exponentiation of tuning possibilities [13,37]. In $SrCoO_{2.5}$ films, a selective insertion of oxygen or hydrogen in the crystal lattice by ionic liquid gating has already been exploited for the switching between ferromagnetic, antiferromagnetic and paramagnetic states [13]. However, the ferromagnetism in this system occurs below room temperature and the switching times are rather long (minutes to hours). For metals with room-temperature ferromagnetism [10,26,38] the combination of hydrogen and oxide/hydroxide-based effects has not been explored so far.

Here, we select Ni as our model system. Ni has a face-centered cubic structure and, for low H concentration, forms an interstitial solid solution with H without destroying the structure. A decrease in the magnetization of Ni upon hydrogen absorption is known from experimental [39] and theoretical [40,41] works and is attributed to partial electron transfer from H to Ni *3d* orbitals [41]. Also, oxide/hydroxide-based electrochemical reactions at the Ni surface are expected to cause effects similar to those observed for Fe [17,29]. To implement such a combined mechanism, we chose an alkaline aqueous electrolyte, which serves as a reservoir for hydrogen and hydroxide ions, and thus can make both hydrogen- and hydroxide-based magneto-ionic mechanisms possible [17,36]. Since Ni and its alloys, e.g., permalloy, exhibit high abundancy and are commercially important room-temperature magnets, voltage control of magnetism in these materials would boost application perspectives.

Nickel-based electrodes are also well explored in electrocatalysis [42], where minimization of overpotentials is sought-after to increase the energy efficiency of an electrochemical reaction. In electrocatalysis, besides choosing a catalytically active electrode material, the use of additives in the electrolyte is an additional strategy to influence overpotentials by promoting or suppressing certain reaction steps or reactions [43,44]. For magneto-ionics, where the electrode materials must meet specific requirements regarding their magnetic properties, the use of electrolyte additives could become an original method to improve reaction kinetics, energy efficiency, and even the magneto-ionic effect strength without modifying the magnetic electrode itself. Few examples have already demonstrated the potential of electrolyte engineering for magneto-ionics [45,46]. For nickel electrocatalysts in alkaline solutions several electrolyte additives are known [47], and thus synergies between the two fields can be readily exploited for the magneto-ionic control of our Ni model system.

In this work, we report a combination of reversible hydrogen- and hydroxide-based effects in electrodeposited, nanocrystalline nickel films. The mechanisms are investigated by using two complementary methods: *in situ* superconducting quantum interference device (SQUID) magnetometry, measuring the absolute magnetic moment, and *in situ* magneto-optical Kerr effect (MOKE) magnetometry, allowing fast measurements of the full hysteresis loop. We find that the addition of thiourea promotes the dual magneto-ionic effect by decreasing the reaction overpotentials and amplifying its magnitude by a factor of 2. With the possibility to operate at low voltage at room temperature, the additive-assisted hydrogen- and hydroxide-based mechanism may initiate a new direction for magneto-ionics in ferromagnetic metals and alloys and thereby expand the range of practical magneto-ionic applications.

II. METHODS

A. Preparation of nickel films

Electrochemical deposition of Ni films was performed on Si/SiO_x wafers with sputter-coated Cr/Ti buffer and Au layers (10–100 nm). Details on the sputtering and Au layer properties can be found in previous work [29]. The Au layer serves as conduction layer for electrodeposition. For the samples used for *in situ* SQUID measurements, the wafer was cut in thin strips and the electrodeposition took place on a predefined area of $4 \times 3\,mm^2$ on these strips. For Kerr microscopy measurements, the electrodeposition took place on a circular area of $38.5\,mm^2$ (as defined by the O-ring sealing the electrochemical cell) on a substrate with an area of $10 \times 10\,mm^2$.

A common all-sulfate-based electrolyte solution for Ni electrodeposition was chosen [48], containing $NiSO_4 \cdot 6\,H_2O$ (100 g/l), H_3BO_3 (45 g/l) and ascorbic acid (1.5 g/l). The pH was 3. The electrochemical cell was a three-electrode setup with a Pt cage as the counter electrode and a saturated calomel

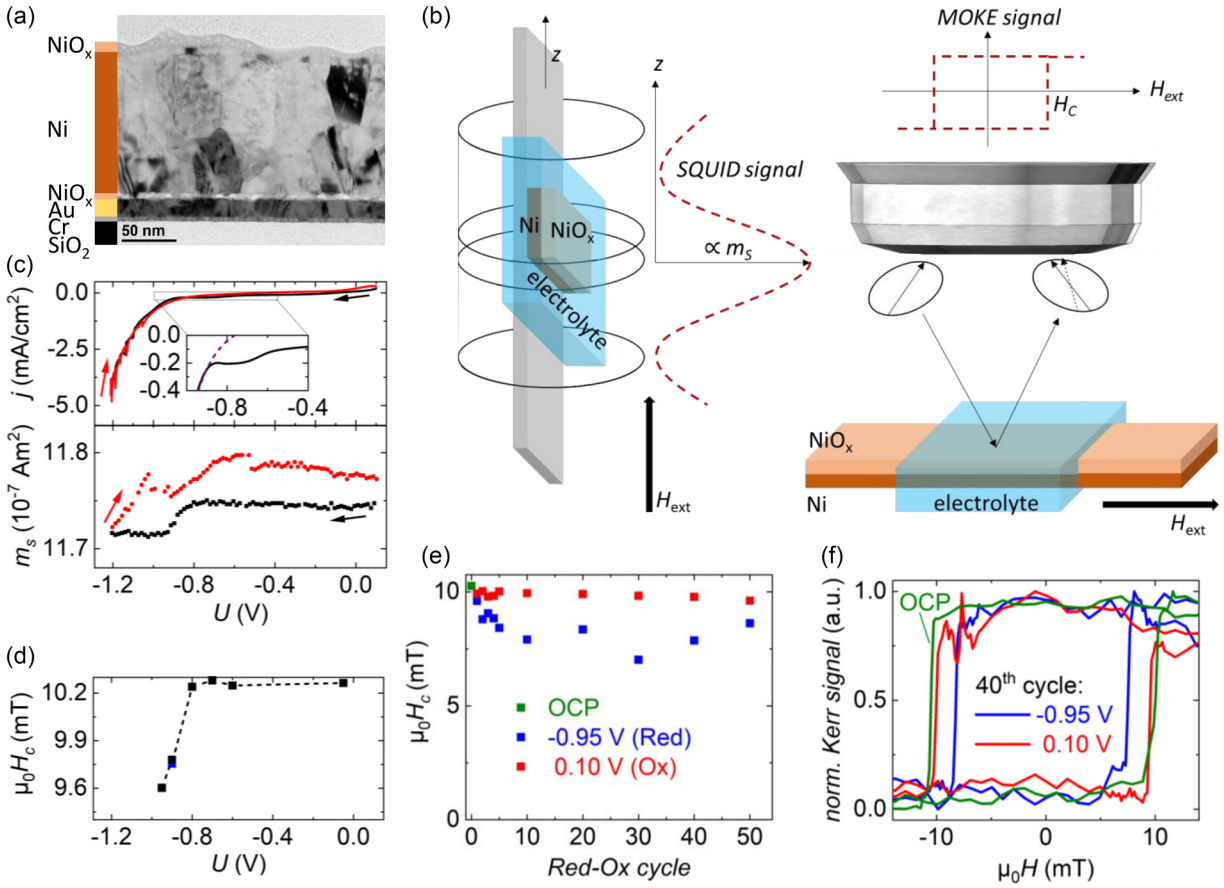


FIG. 1. Dual hydrogen- and hydroxide-based ionic control of magnetism in Ni films. (a) Cross-sectional HR-TEM image of the Ni film shows nanosized grains and a thin oxide surface layer. (b) *In situ* SQUID magnetometry (left scheme) was used to measure the magnetic moment, while *in situ* MOKE (right scheme) was used to measure the hysteresis loops of Ni films during the electrochemical polarization. (c) *In situ* SQUID-CV of a Ni film with a scan rate of 1 mV s^{-1} in 0.5 M KOH solution at a magnetic field of $\mu_0 H = 0.5$ T. The arrows indicate the direction of the cathodic (black) and anodic (red) half cycles. The current density j at very negative potentials (upper panel) is characteristic for water reduction. In the inset, the cathodic half cycle as well as an exponential extrapolation of the water reduction current are shown as full and dashed lines, respectively. Coinciding with the start of water reduction, a decrease of m_s by 0.3% (lower panel) is observed. (d) Coercivity of a Ni film in 0.5 M KOH as a function of reducing potential measured via *in situ* MOKE magnetometry. (e) Switching between low- and high-coercivity states upon application of alternating reduction (–0.95 V) and oxidation potentials (0.1 V). (f) Hysteresis loops for OCP state and the 40th reduction and oxidation cycle from (e).

electrode (SCE) as the reference electrode. The samples were deposited in potentiostatic mode at a deposition potential of –0.9 V_{SCE}, the deposition time was 5 min. This resulted in film thicknesses in the range of 100 to 200 nm, depending on the cell geometry used. High-resolution transmission electron microscopy (HR-TEM) revealed nanocrystalline Ni thin films with columnar Ni grains with a lateral size of around 40 nm [Fig. 1(a)]. The surface is covered with an approximately 5-nm-thick native oxide layer [Fig. 1(a) and Fig. S1 within the Supplemental Material [49]]. Figure 1(a) and S1 also indicate a few nanometers thick oxygen-containing interface layer between the bottom Au layer and the Ni film. The nanocrystalline microstructure is favorable for magneto-ionic applications, as grain boundaries and defect-rich zones can promote the ion transport and H diffusion in Ni films [56].

B. Microstructural and compositional characterization

HR-TEM was conducted on an aberration-corrected Titan^3 80–300 TEM instrument (ThermoFisher Company, USA) to investigate the film layer architecture and microstructure. The preparation of the cross-section lamella was carried out via a focused ion beam technique in FEI Helios Nanolab 600i with Ga^+ ions under conditions of 30 kV and 65 nA.

Raman spectra were recorded on a T64000 triple spectrometer (Jobin Yvon Horiba), equipped with a diffraction grid of 600 g mm^{-1} and a 532-nm excitation wavelength of a Torus 532 laser (Laser Quantum). An UMPlanFLN 20XW Olympus water immersion objective was used for both *ex situ* and *in situ* measurements. The *in situ* Raman measurements were carried out in a two-electrode electrochemical cell. To approximately relate the two-electrode potentials to the three-electrode potentials, conversion measurements in a three-electrode electrochemical cell were carried out by additionally measuring the two-electrode potential.

C. Electrochemical conditions for magneto-ionic switching

The voltage control of magnetism in Ni films was investigated in 0.5 M KOH solutions (pH = 13.85) and in 0.5 M

KOH with thiourea additive (1 g/l). The Ni film served as the working electrode and a Pt wire as the counter electrode. In case of three electrode measurements, a Pt wire was the quasireference electrode. In the following, potentials are generally quoted vs a Pt reference electrode unless mentioned otherwise.

All cyclic voltammograms (CV) started and ended at the initial open circuit potential (OCP). We switched between suitable reduction and oxidation potentials in a range from –1.2 V to 0.1 V vs Pt. For selected cases, potentiostatic switching procedures between reduction and oxidation potentials were performed.

D. (*In situ*) magnetic characterization

For the measurements in the SQUID magnetometer (MPMS-XL-7, Quantum Design), an electrochemical cell design according to Ref. [57] was used. The working principle of *in situ* SQUID magnetometry is schematically drawn in Fig. 1(b). The sample is gradually moved through a second-order gradiometer coil along its z axis, which is coupled to the SQUID detector. The detector picks up a voltage signal as a function of z, which is characteristic for this coil arrangement. The magnetic moment, in our case the saturation moment m_s, for each data point can be calculated from the peak height of the SQUID signal. The Ni films were deposited on the substrate before the electrochemical cell assembly. The Ni thin film was contacted as the working electrode via the Au underlayer, while Pt wires served as counter- and reference electrodes. A sketch of the gating geometry is provided Fig. S2a within the Supplemental Material [49]. Further details on the electrochemical cell can be found in Ref. [57]. The measurements of magnetic saturation moment m_s were performed at a temperature of 300 K and in a magnetic field of 0.5 T. The hysteresis measurement (Fig. S3 within the Supplemental Material [49]) shows that at this magnetic field the films are in saturated state, the coercivity (H_c) lies at a much smaller field of 8.5 mT. An Autolab PGSTAT204 potentiostat (Metrohm) was used to simultaneously apply the potential and perform the electrochemical measurements. A series of measurement routines was applied to the samples, always starting and ending at OCP. For measurements with 0.5 M KOH solution as electrolyte, we performed two CV cycles. For the measurements with 0.5 M KOH with thiourea as the electrolyte, we performed two CV cycles and then additional potentiostatic switching procedures with different step durations of 7 min, 2 min, and 1 min. The data obtained during potentiostatic switching experiments are plotted with regard to the relative time t, with $t = 0$ set as the first data point in the graph.

In the Kerr microscope setup, also shown in Fig. 1(b), the selective sensitivity was set to pure in-plane magnetization using the longitudinal magneto-optical Kerr effect (MOKE) [58]. An external magnetic field was applied in the sample plane parallel to the incident light. For MOKE magnetometry, the Kerr intensity of a selected sample area was plotted as a function of magnetic field [59]. *In situ* MOKE measurements were carried out in a three-electrode electrochemical cell with a cover glass, which was specially built in house to be compatible with the microscope. Details on this *in situ* Kerr microscope setup can be found in previous work [22]. As in the in situ SQUID cell, the Ni film is contacted via the Au underlayer (see Fig. S2b within the Supplemental Material [49]). To account for the different refractive indices of the cover glass and the electrolyte, a long-distance objective (Zeiss LD Neofluar with 20× magnification) with a collar ring was used to focus on the sample surface. The measured hysteresis loops were normalized and corrected for drift and Faraday effects in the objective lens and the cover glass. The magnetic hysteresis loops were measured *in situ* at OCP and subsequently during the application of reduction and oxidation potentials, in the latter cases 5 min after the start of the application of the potential.

E. Density functional theory calculations

The presented density functional theory (DFT) results were obtained with the full-potential local-orbital (FPLO) code [60], version 18.00–52 [61], by employing the PBE implementation [62] of the generalized gradient approximation (GGA). Integrations in reciprocal space were carried out with a linear tetrahedron method including Blöchl corrections on a mesh of 24 × 24 × 24 intervals in the full Brillouin zone. Hydrogen was considered to be situated at octahedral sites, since this interstitial position was found to be more than 0.1 eV lower in energy than the tetrahedral position in a recent GGA calculation [41]. As a minimum structure model for NiH_x, a simple cubic cell (space group 221) with four nickel atoms at the positions $1a$ (0, 0, 0) and $3c$ (1/2, 1/2, 0) was used, including four octahedral positions. The latter were left empty ($x = 0$) or occupied with one hydrogen atom at the position $1b$ (1/2, 1/2, 1/2) for the case $x = 0.25$ (Ni_4H) or occupied with three hydrogen atoms at $3d$ (1/2, 0, 0) for $x = 0.75$ (Ni_4H_3). Scalar relativistic calculations were conducted with the assumption of a ferromagnetic alignment of the Ni moments and with optimization of the lattice parameter.

III. RESULTS AND DISCUSSION

A. Dual hydrogen- and hydroxide-based magneto-ionics in Ni films

To monitor the magnetic moment of nickel films upon electrochemical treatment, we employed cyclic voltammetry (CV) measurements combined with *in situ* SQUID magnetometry. In the CV, the potential was cycled in the range between –1.2 V and 0.1 V at a low scan rate of 1 mV/s in order to resolve slow ion-specific processes. The lower potential limit of –1.2 V was selected in order to exceed the potential of water reduction (–0.8 V), as a prerequisite for hydrogen absorption in the Ni film. Current density j and magnetic saturation moment m_s were recorded simultaneously and are plotted in the upper and lower graph of Fig. 1(c), respectively. Results are shown for the second cycle (both cycles are shown in Fig. S4 within the Supplemental Material [49]).

In the cathodic scan in Fig. 1(c), a current peak is first observed at around $U = –0.7$ V. Between potentials of around –0.8 V and –0.95 V, an abrupt decrease of m_s is detected. We quantify the magnetic moment decrease to $\Delta m_s = (3.3 \pm 0.5) \times 10^{-9}$ Am^2, which corresponds to a relative change of 0.3%, by using the averaged moment values obtained from 10–15 points in the CV regions where m_s is plateau-like before

and after the decrease. This decrease of m_s coincides with the onset of a strong cathodic current increase. In the further course, between –0.95 V and –1.2 V, m_s reaches a plateau, while the cathodic current density further increases. After reversal of the potential scan direction, m_s increases up to U = –0.6 V with values exceeding the initial m_s by 0.4%. The cathodic current density continuously decreases and eventually becomes anodic. The same features also occur in the preceding cycle (Fig. S4 within the Supplemental Material [49]), with a shift related to the different starting value for m_s. In the following, the interpretation of our *in situ* magnetometry results is guided by extensive previous literature [56,63,64] describing the electrochemical behavior of Ni electrodes in alkaline solutions.

Prior to immersion in the electrolyte, under ambient conditions, a few nanometer thin α-Ni(OH)$_2$/NiO$_x$ bilayer is expected on the Ni surface [56]. When immersed into aqueous KOH solution, a thinner NiO$_x$ layer is found, implying further conversion to nickel hydroxide [63]. Over time in the KOH solution, the α-Ni(OH)$_2$ layer is known to successively convert into the more stable β-Ni(OH)$_2$ phase in a process known as chemical ageing [65,66]. As this phase transformation is slow in neutral and dilute alkaline solutions at room temperature [65], we expect a mixed coverage of NiO$_x$ and both the α-Ni(OH)$_2$ and the β-Ni(OH)$_2$ phase as a thin layer on our sample surface in the KOH electrolyte at the open-circuit potential (OCP). We examined the surface structure of our Ni films in *ex situ* state and at OCP in the KOH solution using *in situ* Raman spectroscopy (see Fig. S5a within the Supplemental Material [49]). We found no signals for α-Ni(OH)$_2$ or β-Ni(OH)$_2$. However, it is well known that Raman spectroscopy usually cannot detect very thin surface layers [56], which also holds true for thin Ni(OH)$_2$ layers [67]. Thus, we still consider a thin layer of mixed surface coverage consisting of both Ni hydroxides and NiO$_x$ as the most likely surface state of our samples at OCP.

When the potential is ramped to more negative values than the OCP in the course of the CV, different electrochemical reactions can occur on the Ni surface according to the literature [56]: (i) the reduction of α-Ni(OH)$_2$/NiO$_x$ to metallic Ni, (ii) the reduction of β-Ni(OH)$_2$ to metallic Ni, and (iii) water reduction, which generates adsorbed hydrogen atoms, which then can recombine to H$_2$ gas and be absorbed into Ni. It is known that the α-Ni(OH)$_2$ species is reduced to metallic Ni at potentials close to the onset of water reduction [56,63]. The β-Ni(OH)$_2$ phase, in contrast, is more stable and reduction of this phase requires more cathodic potentials [56]. In our CV, in line with previous studies [56,63], we assign the small cathodic current peak close to –0.7 V to the reduction of a small amount of α-Ni(OH)$_2$ to metallic Ni. The strong cathodic current density increase at around –0.9 V is caused by water reduction. While the major part of the water reduction current density is consumed for adsorbed hydrogen atoms recombining to gaseous H$_2$, a minor fraction of it is associated with adsorbed hydrogen atoms that are subsequently absorbed. Considering the overlap with the current density peak at more positive potentials, we infer that the onset of water reduction lies around –0.8 V, see the extrapolation of the water reduction current density in the inset of Fig. 1(c).

We can now proceed to ascribe changes in m_s during the CV [Fig. 1(c), lower panel] to electrochemical reactions. The magnetic saturation moment remains constant in the potential region down to –0.7 V, in which no electrochemical reactions occur according to the CV [Fig. 1(c), top]. We can conclude that electrochemical double layer charging, which is the only process occurring in this first potential region of the CV, does not induce measurable changes of m_s. The decrease of m_s observed between –0.8 V and –0.9 V in the cathodic scan lies in the potential range where the start of both hydrogen absorption and α-Ni(OH)$_2$ reduction is expected from the current response. Thus, the measured net m_s is likely a superposition of both processes. According to DFT calculations (see Fig. S6 within the Supplemental Material [49]), hydrogen absorption into Ni can explain a decrease in m_s. In contrast, the electrochemical reduction of paramagnetic nickel hydroxide [68] to ferromagnetic Ni would yield an increase in m_s. We conclude that any increase in magnetic moment due to the reduction of a small amount of α-Ni(OH)$_2$ at the surface is masked by the stronger decrease in m_s because of hydrogen absorption. Adsorbed hydrogen atoms might also contribute to the decrease in m_s, [69] but could only account for a fraction of the total m_s decrease as elaborated in Note S1 at the end of the Supplemental Material [49]. When the potential is ramped below –0.9 V, m_s reaches a plateau, indicating that the hydrogen concentration in the Ni film remains constant [64]. The observed plateau in m_s also rules out that H$_2$ gas evolution effects influence the measured m_s response, because such effects would become more prominent when scanning to more negative potentials with higher H$_2$ gas evolution rate [Fig. 1(c), top].

From DFT calculations (see Fig. S6 within the Supplemental Material [49]) we can conclude that m_s is expected to decrease linearly with growing hydrogen content in the Ni lattice, as also shown in Ref. [41], where an extended structure model was used. We can use this linear relationship to estimate the H/Ni ratio needed for a reduction of m_s by 0.3%, as observed in the CV. This calculation yields a value of 0.003 H/Ni. Previously, hydrogen concentrations in the order of H/Ni = 0.01 have been reported for hydrogen absorption into Ni thin films from KOH solution, based on strain measurements [64]. In our case, the possible superposition of α-Ni(OH)$_2$ reduction would lead to a smaller net decrease of m_s. Therefore, our H/Ni ratio represents a lower limit and actual values could approach values from the preceding publication [64].

Upon reversal of the scan direction at –1.2 V, we first observe an increase in m_s. For the reverse process of hydrogen desorption from the Ni films, an increase in m_s is naturally expected. Somewhat surprisingly, however, the observed increase of m_s commences instantly at the potential turnaround in the anodic scan direction. We hypothesize that the reduction of β-Ni(OH)$_2$ to ferromagnetic Ni, which is known to occur at very negative potentials, well in the region of hydrogen evolution [56], could be responsible for this increase of m_s. While an unambiguous assignment cannot be made at this point, we can speculate that the onset of β-Ni(OH)$_2$ reduction may be connected to a changing hydrogen gas evolution rate or hydrogen surface coverage at that point. Recently, a voltammetric protocol using slow scan rates $\leqslant 1\,\mathrm{mVs}^{-1}$, similar to

our *in situ* CV procedure, has been proposed for the reduction of β-Ni(OH)$_2$ in the literature [70], where this reduction could also be achieved in the anodic scan direction.

Assuming that the increase of m_s in the anodic scan below -1.0 V ($\Delta m_s = 5 \times 10^{-9}$ Am^2) is solely due to the β-Ni(OH)$_2$ reduction reaction, one can estimate an average thickness of the newly formed Ni layer to be 0.8 nm (see Note 2 at the end of the Supplemental Material [49]). For Fe thin films it has been found that about 1.5 nm of iron is consumed by a native oxide layer of a 3–4-nm thickness [71], that can also be (partially) recovered upon electrochemical reduction. Considering the expectation of a mixed coverage of our surface with both hydroxide phases, an average thickness increase of the Ni layer by 0.8 nm upon reduction of the β-Ni(OH)$_2$ appears possible.

In the further course of the reverse scan, when the potentials become more positive than the onset of water reduction ($U >$ –0.8 V), the further increase in m_s can be assigned to the hydrogen desorption process. The net moment increase beyond the initial m_s value in the reverse scan can thus be explained by a combined effect based on both hydrogen desorption and hydroxide reduction. From approximately –0.6 V on, m_s slowly decreases again, which agrees with the expected re-oxidation of metallic nickel to nickel oxide-hydroxide [56]. The increase of m_s over the initial value (by 0.4%) at $U >$ –0.6 V indicates that the nickel oxide, hydroxide, or oxy-hydroxide layer formed by electro-oxidation consumes less nickel than the air-formed native oxide. This has been found in a similar manner for iron-based magneto-ionic systems [22].

For a further investigation of the combined hydrogen- and hydroxide-based magneto-ionic effect, we study changes in coercivity upon electrochemical switching using *in situ* MOKE magnetometry [Figs. 1(d)–1(f)]. Although this technique [schematically shown in Fig 1(b), right] does not yield quantitative information on the magnetic moment, it allows us to probe the full magnetic hysteresis within seconds. This makes it an ideal complement to SQUID magnetometry, which can measure absolute values for the moment on longer timescale. The hysteresis measured after the Ni film is immersed in the electrolyte, at OCP, is similar to the hysteresis of the pristine state (not shown). This confirms that the sole addition of electrolyte does not induce magnetic property changes. Using *in situ* MOKE, we measured hysteresis loops at constant potentials, with a stepwise change toward more negative potentials. When reduction potentials $\leqslant -0.9$ V are applied, a significant decrease in H_c is found [Fig. 1(d)]. We demonstrate that this coercivity decrease is reversible by applying reduction and oxidation potentials (–0.95 V and 0.1 V) alternatingly for 50 Red-Ox cycles [Fig. 1(e)]. The relative coercivity change ΔH_c, defined with respect to the coercivity of the oxidized state in each Red-Ox cycle, increases up to almost 30% with higher cycle numbers [Fig. 1(e)]. Hysteresis loops for the OCP state, as well as the 40th Red-Ox cycle [Fig. 1(f)] show that the shape of the original hysteresis loop is restored upon oxidation.

The coercivity decrease upon application of –0.9 V occurs at a potential at which both hydrogen absorption and α-Ni(OH)$_2$ reduction are expected to occur. While the observed decrease in magnetic moment at this potential could be unambiguously attributed to hydrogen absorption, it is not straightforward to assign the decrease in coercivity to either one of the two, or both electrochemical reactions. Previous reports have shown that hydrogen can affect the coercivity of Ni [39,72], although it is unclear whether this is due to intrinsic (anisotropy [73]) or extrinsic factors (microstructure and pinning sites [72]). On the other hand, the observed coercivity decrease upon application of a reduction potential could also be related to the removal of surface oxides/hydroxides, which can act as pinning site for domain walls [29]. Upon reduction at –0.9 V, α-Ni(OH)$_2$/NiO$_x$ can transform into ferromagnetic nickel, which could unpin domain walls from the oxide/hydroxide phases and therefore lead to a decrease in H_c. This mechanism has already been proposed for a voltage-induced decrease in coercivity upon reduction in FeO$_x$/Fe systems in alkaline electrolyte [29].

The presented results in this section indicate that in the Ni system in alkaline electrolyte, both, hydrogen- and hydroxide-based magneto-ionic effects are active as a dual magneto-ionic mechanism. On the basis of *in situ* SQUID-CV measurements, we can ascribe magnetic signatures to hydrogen- and hydroxide-based magneto-ionic mechanisms. At reducing potentials, electrochemical hydrogen absorption first leads to a decrease of m_s, while upon reversal of the potential scan direction an increase m_s is observed, which can be explained by combined hydrogen- and hydroxide-based magneto-ionic mechanisms.

B. Promoting hydrogen magneto-ionics by addition of thiourea

Here, we investigate the influence of an electrolyte additive on the magneto-ionic performance of the Ni film system in the same alkaline electrolyte solution as used in the previous section.

It is well known that the efficiency of electrochemical hydrogen absorption in Ni can be increased by using additives in the electrolyte [47,74]. We chose to study the impact of thiourea addition to the alkaline KOH electrolyte solution on the magneto-ionic performance of our Ni films. For that purpose, we carried out *in situ* SQUID and *in situ* MOKE magnetometry experiments for an electrolyte containing thiourea, see Fig. 2. We show the second CV cycle in the electrochemical SQUID cell in Fig. 2(a), in analogy to our measurements in the pure KOH electrolyte [Fig. 1(c), shown again as faint lines in Fig. 2(a)]. In the electrolyte solution containing thiourea, the cathodic current related to reduction of water arises at an overpotential $\sim$0.25 V smaller compared to the KOH electrolyte solution. This decrease in overpotential indicates a catalytic effect of thiourea on water reduction, and consequently, hydrogen absorption.

Considering changes in m_s, we observe a decrease by $\Delta m_s = (6.5 \pm 0.2) \times 10^{-9}$ Am^2, which corresponds to a relative change of 0.5%, in the cathodic scan in the CV. This corresponds to an enhancement by a factor of 2.0 ± 0.4 compared to measurements in pure KOH solution in Fig. 1(c), i.e., twice the absolute moment change. Again, m_s exceeds its initial value after potential reversal in the anodic scan. However, this time, the increase does not start immediately at the reversal point ($U =$ –1.2 V), but occurs at more positive potentials. We attribute the overall behavior to an analogous dual-ionic mechanism as described above for the Ni film

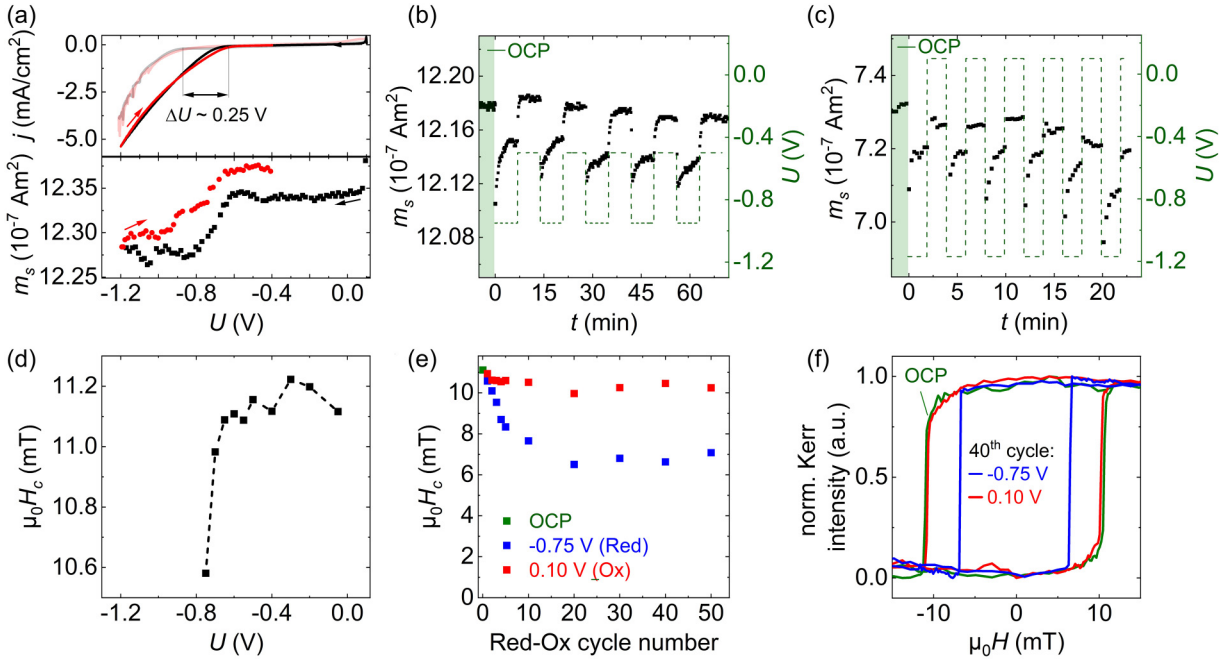


FIG. 2. Thiourea-assisted dual-ionic control of magnetism in Ni. *In situ* SQUID and MOKE measurements on Ni films are performed in 0.5 M KOH solution with 1 g/L thiourea. (a) *In situ* SQUID-CV of a Ni film with a scan rate of 1 mVs^{-1} at a field of $H = 0.5$ T (black and red lines) compared with the CV in pure 0.5 M KOH solution (faint black and red lines). The arrows indicate the cathodic (black) and anodic (red) half cycles. With thiourea addition, current density j and magnetic saturation moment m_s decrease at less negative potentials. (b), (c) Magnetic saturation moment (black) upon application of constant potentials (green dashed lines) of (b) –0.95 V and –0.5 V with a holding time of 7 min for each step and (c) –1.17 V and 0.1 V with a holding time of 2 min for each step. The data is obtained after holding the sample at OCP, following prior in situ switching procedures (see Fig. S7 within the Supplemental Material [49]). A reversible switching of up to 4% of m_s is demonstrated in (c). Note that the difference in the absolute m_s values for (b) and (c) stems from different film thicknesses. (d) Coercivity of a Ni film in 0.5 M KOH solution with 1 g/L thiourea as a function of potential measured via *in situ* MOKE magnetometry. (e) Switching between low- and high-coercivity states upon application of alternating reduction (–0.75 V) and oxidation potentials (0.1 V). Note that the coercivity reduction also occurs at less negative potentials compared to the pure KOH electrolyte (–0.75 V vs –0.95 V). (f) Hysteresis loops for the 40th reduction and oxidation cycle from (e).

in KOH, here initiated at less negative potentials. The latter aspect is generally favorable for the energy efficiency of magneto-ionic devices. We will discuss later in the paper how the presence of thiourea could be responsible for the earlier and stronger initial drop in m_s, which indicates an improved hydrogen absorption into Ni.

At this point, in order to explore the reversibility of the improved magneto-ionic switching of m_s in the thiourea-containing electrolyte, we performed a series of potentiostatic switching experiments in the SQUID magnetometer. After two CVs, we applied potentials of –0.95 V and –0.5 V alternatingly for 7 min. In Fig. 2(b), we illustratively show the m_s changes observed during switching cycles started after a pause at OCP and 65 prior switching cycles. An abrupt decrease of m_s of about 0.5% is detected at potentials of –0.95 V, which we ascribe to hydrogen absorption. The switching time for the initial decrease is less than 10 seconds for this process, likely only limited by the temporal resolution of the SQUID magnetometer. The diffusion coefficient of H in electrodeposited nanocrystalline Ni is reported to be 3×10^{-12} m^2 s^{-1} [75], thus H should be able to diffuse through the whole film thickness within milliseconds. Therefore, we expect the hydrogen concentration within the film to be constant and saturated within this first reduction step. In the same potential step at larger times, m_s starts to increase, which is a signature of hydroxide reduction. Upon oxidation at the potential of –0.5 V, the magnetic moment rapidly increases and approximately reaches the value at OCP again. This can be explained by desorption of hydrogen along with simultaneous re-oxidation of the metallic Ni, which are both expected to proceed at this potential. Figure S7a within the Supplemental Material [49] shows that similar characteristics are observed for preceding cycles, although a drift in overall m_s becomes apparent towards later cycles. Pursuing this testing scheme on another sample, we recorded changes in m_s upon periodic switching in the larger voltage range between potentials of –1.17 V and 0.1 V with shorter holding times of 2 minutes per step for 15 cycles and of 1 minute per step for 10 cycles, (Fig. S7b within the Supplemental Material [49]). Figure 2(c) illustratively shows cycles 5–10 for the holding times of 2 min, started after a pause at OCP. At the cathodic potential of –1.17 V, an abrupt decrease by about 4% of m_s is observed, which is followed by a slower increase of m_s over time. At the oxidation potential of 0.1 V, a rapid increase of m_s is again observed. The evolution of m_s during the voltage steps is thus similar to that in Fig. 2(b), and this is also found for switching with holding times of 1 min (Fig. S7b within the Supplemental Material [49]). The procedures confirm that reversible magneto-ionic switching of m_s can be achieved.

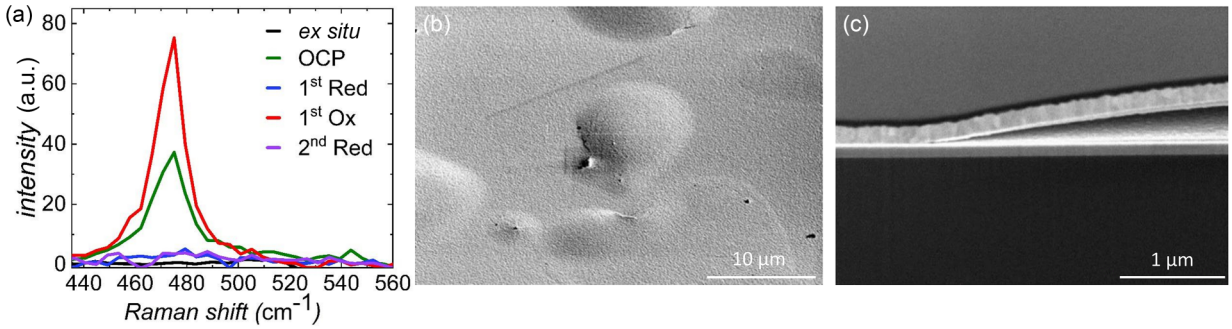


FIG. 3. Thiourea-assisted hydrogen absorption in nickel films. (a) Selected range of the Raman spectra of the nickel film in as deposited (*ex situ*) state and in the OCP state and at reduction (Red) and oxidation (Ox) potentials in thiourea-containing KOH electrolyte solution. The peak associated with α-Ni(OH)$_2$ vanishes/reappears upon reduction/oxidation. The background is subtracted to facilitate comparison of the peaks. As collected, extended spectra are given in Fig. S5b within the Supplemental Material [49]. (b), (c) SEM images of the surface and cross section of the Ni film after five Red-Ox cycles show bubble-like delamination areas.

As for the pure KOH electrolyte, we also investigated magneto-ionic effects using *in situ* MOKE magnetometry. Changes in H_c in Figs. 2(d)–2(f) upon application of oxidation and reduction potentials in 0.5 M KOH electrolyte with thiourea additive show the same tendency as in the case of the pure KOH electrolyte solution. However, in the presence of the thiourea additive, such switching is observed at a smaller cathodic potential (–0.70 V, compared to the –0.90 V for pure KOH), which is analogous to the observations for the m_s changes. A relative variation of coercivity between oxidized and reduced states, ΔH_c, of around 30% is attained with higher Red-Ox cycle numbers [Figs. 2(e) and 2(f)], equaling the value obtained for the KOH electrolyte solution without thiourea. On another sample, we confirmed that such large coercivity changes can be achieved even during a prolonged switching routine of up to 1000 Red-Ox cycles, without notable degradation of the magnetic properties or surface morphology (see Fig. S8 within the Supplemental Material [49]).

To elucidate the origin of the amplified magneto-ionic response and the lower overpotentials from the addition of thiourea, we characterized the surface state of the Ni thin films in the electrolytes using *in situ* Raman spectroscopy. Figure 3(a) shows a peak at around 475 cm^{-1} in the Raman spectrum of the nickel films with the thiourea-containing electrolyte, which we attribute to α-Ni(OH)$_2$ [76–78]. It is clearly seen that the peak is initially absent, but appears with the addition of the electrolyte at OCP. Upon application of a reducing potential, the α-Ni(OH)$_2$ peak disappears, which is in line with the expected reduction of α-Ni(OH)$_2$ to metallic nickel [56]. Subsequent application of an oxidation potential leads to the reappearance of this peak. During a second application of a reduction potential, the peak vanishes again, which shows that this process is reversible. Potentials used in this two-electrode experiment (given in Fig. S5 within the Supplemental Material [49]) roughly correspond to the three-electrode reduction/oxidation potentials used in Fig. 2(e). Importantly, in the system without thiourea, this nickel hydroxide peak was not observed (Fig. S5a within the Supplemental Material [49]). This evidences that α-Ni(OH)$_2$ is stabilized in the presence of thiourea, yielding a sufficiently thick layer detectable by *in situ* Raman spectroscopy. The atomistic mechanism for stabilization cannot be resolved at this point. However, an enhanced stability of the α-Ni(OH)$_2$ phase compared to the β-Ni(OH)$_2$ phase has also previously been reported for hydroxide nanoparticles in alkaline solution in the presence of thiourea as an additive [79].

Presumably, this surface modification with α-Ni(OH)$_2$ contributes to the improved hydrogen absorption in our Ni thin film. Thiourea has been used as a promoter for hydrogen absorption into Ni electrodes in both acidic [47,80] and alkaline [81] solutions, while it has also been found that an increasing thickness of a Ni(OH)$_2$ layer on the nickel surface benefits hydrogen absorption in alkaline solution [82]. The improved hydrogen absorption caused by the addition of thiourea in our experiments even leads to characteristic bubble-like delamination areas between the hydroxide-covered Ni film and the substrate after electrochemical treatment [Figs. 3(b) and 3(c)]. Bubble-like delamination typically occurs when hydrogen gas bubbles form on the bottom side of the film during hydrogen desorption and can be considered a characteristic feature of prior hydrogen absorption into thin films [26]. These features have not been observed for Ni films in the pure KOH electrolyte solution.

Furthermore, the surface modification by α-Ni(OH)$_2$ may explain the smaller overpotentials needed for a magneto-ionic effect in the presence of thiourea, as evidenced in both *in situ* SQUID and *in situ* MOKE magnetometry experiments in electrolytes with and without thiourea [Figs. 1(c), 1(d), 2(a), and 2(d)]. Previous studies demonstrated a significant catalytic effect of nickel hydroxide on the hydrogen evolution reaction (HER) in an alkaline medium [83–85]. Especially α-Ni(OH)$_2$ surfaces are found to decrease the overpotential for the HER significantly [85], which aligns with our Raman results pointing at α-Ni(OH)$_2$ as the predominant species on our Ni films in the electrolyte with thiourea. Since hydrogen adsorption resulting from water reduction is the first elementary step required for both the HER and the hydrogen absorption, a catalytic effect on hydrogen absorption is similarly expected. Therefore, we ascribe the decrease in overpotential of ~0.25 V with thiourea observed in the current curves [Fig. 2(a)] as well as in our magneto-ionic measurements to the catalytic effect of α-Ni(OH)$_2$.

To complete the picture, another notable difference between electrolyte with and without thiourea can be related to

the hydroxide species on the surface. In our *in situ* SQUID magnetometry experiments, we observe a pronounced increase in m_s directly upon reversal of the scan direction at –1.2 V in pure KOH in Fig. 1(c), while such an increase is absent in the analogous experiment with thiourea as an additive in Fig. 2(a). This hints at a smaller amount of β-$Ni(OH)_2$ on the surface of the Ni film in the electrolyte with thiourea, as the increase in m_s at that potential in KOH was ascribed to the reduction of β-$Ni(OH)_2$. Our finding of a surface-dominating α-$Ni(OH)_2$ species on the Ni film in solution with thiourea from the Raman experiments supports this interpretation.

Finally, we return to a comparison of the overall magneto-ionic performance of Ni thin film electrodes with and without thiourea. Comparing the hydrogen-based magneto-ionic performance of the thiourea-containing KOH solution (Fig. 2) with the pure KOH electrolyte (Fig. 1), one observes a marked increase in the variation of m_s upon hydrogen absorption in the CV with thiourea, which is twice the value compared to the pure KOH solution. In potentiostatic switching mode we even achieve up to 4% relative variation of m_s with thiourea addition. Coercivity is decreased upon application of reduction potentials by up to 30%, which is not significantly affected by the addition of thiourea. This might be an indication that the main cause for the coercivity reduction is not the promoted hydrogen absorption, but the reduction of α-$Ni(OH)_2/NiO_x$ on the surface, which is expected on the surface in electrolytes with and without thiourea. Furthermore, a coercivity increase, as opposed to the observed decrease, is expected for hydrogen absorption into Ni from previous work on Ni foils [39]. The magnetic mechanism for an increased coercivity in the oxidized state would remain similar whether involving NiO_x or α-$Ni(OH)_2$ on the surface, as both can act as pinning sites for magnetic domain walls, similar to FeO_x [29].

IV. CONCLUSIONS

In this work, we have demonstrated the possibility of a reversible dual magneto-ionic control in ferromagnetic nickel films by a combined hydrogen- and hydroxide-based mechanism. We have shown that the hydrogen-based mechanism can be enhanced by adding thiourea to the electrolyte solution. Remarkably, thiourea addition promotes not only the energy efficiency of the observed magneto-ionic effect by decreasing the required overpotential, but also amplifies the magnitude of the magnetization changes by a factor of 2 by enhancing hydrogen absorption into the nickel film.

Based on *in situ* SQUID magnetometry, *in situ* MOKE magnetometry and *in situ* Raman spectroscopy data we have attributed the magneto-ionic effects in Ni films in a KOH electrolyte to both hydrogen- and hydroxide-based reactions. Hydrogen has been found to reduce the magnetic moment in Ni as a result of hydrogen absorption, which is supported by DFT calculations. An enhancement of the magnetic moment can be explained by the reduction of a surface oxide or hydroxide species and the hydrogen desorption process, which act as a dual-ion magneto-ionic mechanism. Coercivity changes could not be unambiguously attributed to either absorption of hydrogen or the reduction of the surface hydroxide/oxide, although the similar magnitude of the coercivity variation with and without thiourea hints at hydroxide/oxide reduction as the cause of the effect. Such a dual hydrogen- and hydroxide/oxide-based magneto-ionic mechanism could provide the key to the independent tuning of coercivity and magnetic moment in magnetic materials.

Our dual hydrogen- and hydroxide-based magneto-ionic control in nickel films could also be transferred to other materials systems. Although pure metals with an affinity to hydrogen are scarce (e.g., Ni, Ti, Pd, Pt), several alloy systems on the basis of these elements (such as Ni-Fe, Fe-Pd) can be considered as candidates for an analogous dual magneto-ionic mechanism.

The disentanglement of hydrogen- and hydroxide-based magneto-ionic mechanisms is desirable from a fundamental point of view, yet inherently difficult for Ni films in alkaline electrolyte, where both processes overlap during the reduction and oxidation steps. The use of acidic electrolyte solutions could suppress the hydroxide-based pathway and enhance the hydrogen-based magneto-ionic control, but problems related to parasitic Ni dissolution and redeposition are likely to occur here. Another possibility is the addition of a hydrogen-permeable layer, such as Pd, on top of Ni. Such a top layer would exclude hydroxide conversions but enable hydrogen-based magneto-ionic control and could possibly even allow quantification of the hydrogen effect on the magnetism of Ni by means of coulometry [35].

We found that the addition of thiourea catalyzes the water reduction reaction, increases the amount of absorbed hydrogen, and enhances amplitude of the hydrogen-based magneto-ionic effect, presumably by stabilizing an α-$Ni(OH)_2$ layer on the Ni surface. Electrolyte additives are rarely considered in magneto-ionic systems, but our results encourage further research in that direction. Especially for hydrogen-based magneto-ionics, the use of additives known to promote hydrogen entry into transition metals, such as compounds containing P, S, As, Se, Sb, or Te [86], may be promising to enhance the kinetics of magneto-ionic effects.

The integration of liquid gating setups into actual electronics may present a challenge. However, integration of liquid gating in a magnetic device for logic functionalities has been demonstrated [87]. Furthermore, minimal amounts of liquid electrolyte are needed in practical devices, which could also be converted into gel forms to prevent leakage. Miniaturization in general is not an issue, as liquid gating strategies can be employed for nanostructures, which typically have a high wettability for electrolytes caused by capillary forces.

Magneto-ionic changes of coercivity were evidenced even after 1000 redox cycles, without significant degradation of magnetic properties or surface morphology. Delamination issues caused by enhanced hydrogen absorption could potentially be a limitation for endurance. The use of layer architectures with stronger adhesion between the magneto-ionic layer and the underlayer or the transfer to 3D structures or free-standing films might be promising alternatives in the future.

ACKNOWLEDGMENTS

This research was co-funded by the European Union's Horizon 2020 research and innovation programme under the Marie Sklodowska-Curie Grant No. 861145, the Deutsche

Forschungsgemeinschaft (DFG, German Research Foundation) (Project No. 499361641) and by the European Union (ERC, ACTIONS, 101125178). The authors thank A. Pöhl for ion beam lamella preparation, J. Zehner for help with *in situ* MOKE measurements, M. Uhlemann for discussions (all Leibniz IFW Dresden), and S. Chokheli (TU Chemnitz) for AFM measurements. All authors gratefully acknowledge the help of M. Hantusch who performed the AES experiments at Leibniz IFW Dresden and provided the experimental details for the description of Fig. S1 in the Supplemental Material. M.R. thanks U. Nitzsche for maintaining the high-performance computing environment at Leibniz IFW Dresden. M.G. and S.T. thank H. Krenn (Institute of Physics, University of Graz) for providing access to the SQUID magnetometer in the framework of the inter-university cooperation of TU Graz and Uni Graz on natural science (NAWI Graz) and R. Würschum (Institute of Materials Physics, Graz University of Technology) for discussion.

M.K. fabricated the samples. M.G. and S.T. carried out *in situ* SQUID magnetometry. *In situ* MOKE was performed by M.K for Figs. 1 and 2 and by M.G. for Fig. S8 within the Supplemental Material. D.W. performed the HR-TEM analysis. M.R. performed the DFT calculations, described their details, created Fig. S6 within the Supplemental Material, and contributed to the revisions of the manuscript. S.S. performed *in situ* Raman experiments together with M.K. and contributed to their interpretation. M.K., M.G., S.T. and K.L. analyzed the experimental data, performed calculations and worked on visualization and conceptualization. M.K. wrote the original draft. K.L. and M.G. revised the original draft and finalized the manuscript. All authors contributed to the writing of the final version of the manuscript.

DATA AVAILABILITY

The data that support the findings of this article are openly available [88].

[1] L. Herrera Diez, D. Chiba, D. A. Gilbert, S. Granville, and K. Leistner, Magneto-ionic and electrostatic gating of magnetism: Phenomena and devices, Appl. Phys. Lett. **123**, 130401 (2023).

[2] C. Leighton, Electrolyte-based ionic control of functional oxides, Nat. Mater. **18**, 13 (2019).

[3] K. Leistner, Electrochemical approaches to room temperature magnetoelectric materials, Curr. Opin. Electrochem. **25**, 100636 (2021).

[4] Y. Gu, C. Song, Q. Wang, W. Hu, F. Pan, and Z. Zhang, Emerging opportunities for voltage-driven magneto-ionic control in ferroic heterostructures, APL Mater. **9**, 040904 (2021).

[5] Y. Liu and G. Yu, MRAM gets closer to the core, Nat. Electron. **2**, 555 (2019).

[6] X. Z. Yu, D. Morikawa, K. Nakajima, K. Shibata, N. Kanazawa, T. Arima, N. Nagaosa, and Y. Tokura, Motion tracking of 80-nm-size skyrmions upon directional current injections, Sci. Adv. **6**, eaaz9744 (2020).

[7] S. Bhatti, R. Sbiaa, A. Hirohata, H. Ohno, S. Fukami, and S. N. Piramanayagam, Spintronics based random access memory: A review, Mater. Today **20**, 530 (2017).

[8] A. Molinari, H. Hahn, and R. Kruk, Voltage-control of magnetism in all-solid-state and solid/liquid magnetoelectric composites, Adv. Mater. **31**, 1806662 (2019).

[9] C. Song, B. Cui, F. Li, X. Zhou, and F. Pan, Recent progress in voltage control of magnetism: Materials, mechanisms, and performance, Progr. Mater. Sci. **87**, 33 (2017).

[10] M. Nichterwitz, S. Honnali, M. Kutuzau, S. Guo, J. Zehner, K. Nielsch, and K. Leistner, Advances in magneto-ionic materials and perspectives for their application, APL Mater. **9**, 030903 (2021).

[11] P. Monalisha, M. Ameziane, I. Spasojevic, E. Pellicer, R. Mansell, E. Menéndez, S. van Dijken, and J. Sort, Magnetoionics for synaptic devices and neuromorphic computing: Recent advances, challenges, and future perspectives, Small Sci. **4**, 2400133 (2024).

[12] M. Nichterwitz, K. Hiekel, D. Wolf, A. Eychmüller, and K. Leistner, Voltage-controlled ON–OFF-switching of magnetoresistance in FeO_x/Fe/Au aerogel networks, ACS Mater. Au **4**, 55 (2024).

[13] N. Lu, P. Zhang, Q. Zhang, R. Qiao, Q. He, H.-B. Li, Y. Wang, J. Guo, D. Zhang, Z. Duan *et al.*, Electric-field control of tri-state phase transformation with a selective dual-ion switch, Nature (London) **546**, 124 (2017).

[14] S. Dasgupta, B. Das, Q. Li, D. Wang, T. T. Baby, S. Indris, M. Knapp, H. Ehrenberg, K. Fink, R. Kruk, and H. Hahn, Toward on-and-off magnetism: Reversible electrochemistry to control magnetic phase transitions in spinel ferrites, Adv. Funct. Mater. **26**, 7507 (2016).

[15] S. Robbennolt, P. Yu, A. Nicolenco, P. Mercier Fernandez, M. Coll, and J. Sort, Magneto-ionic control of magnetism in two-oxide nanocomposite thin films comprising mesoporous cobalt ferrite conformally nanocoated with HfO_2, Nanoscale **12**, 5987 (2020).

[16] M. Nichterwitz, S. Honnali, J. Zehner, S. Schneider, D. Pohl, S. Schiemenz, S. T. B. Goennenwein, K. Nielsch, and K. Leistner, Control of positive and negative magnetoresistance in iron oxide–iron nanocomposite thin films for tunable magnetoelectric nanodevices, ACS Appl. Electron. Mater. **2**, 2543 (2020).

[17] K. Duschek, A. Petr, J. Zehner, K. Nielsch, and K. Leistner, All-electrochemical voltage-control of magnetization in metal oxide/metal nanoislands, J. Mater. Chem. C **6**, 8411 (2018).

[18] X. Ye, H. K. Singh, H. Zhang, H. Geßwein, M. R. Chellali, R. Witte, A. Molinari, K. Skokov, O. Gutfleisch, H. Hahn, and R. Kruk, Giant voltage-induced modification of magnetism in micron-scale ferromagnetic metals by hydrogen charging, Nat. Comm. **11**, 4849 (2020).

[19] M. Prasch, R. Würschum, and S. Topolovec, Indirect magneto-ionic effect in $FeSi_2$/Si nanocomposite induced by electrochemical lithiation and delithiation, J. Phys. Mater. **7**, 03LT03 (2024).

[20] U. Bauer, L. Yao, A. J. Tan, P. Agrawal, S. Emori, H. L. Tuller, S. van Dijken, and G. S. D. Beach, Magneto-ionic control of interfacial magnetism, Nat. Mater. **14**, 174 (2015).

[21] D. A. Gilbert, J. Olamit, R. K. Dumas, B. J. Kirby, A. J. Grutter, B. B. Maranville, E. Aarenholz, J. A. Borchers, and K. Liu,

Controllable positive exchange bias via redox-driven oxygen migration, Nat. Commun. **7**, 11050 (2016).

[22] J. Zehner, R. Huhnstock, S. Oswald, U. Wolff, I. Soldatov, A. Ehresmann, K. Nielsch, D. Holzinger, and K. Leistner, Nonvolatile electric control of exchange bias by a redox transformation of the ferromagnetic layer, Adv. Electron. Mater. **5**, 1900296 (2019).

[23] S. Robbennolt, E. Menendez, A. Quintana, A. Gomez, S. Auffret, V. Baltz, E. Pellicer, and J. Sort, Reversible, electric-field induced magneto-ionic control of magnetism in mesoporous cobalt ferrite thin films, Sci. Rep. **9**, 10804 (2019).

[24] M. Nichterwitz, S. Neitsch, S. Röher, D. Wolf, K. Nielsch, and K. Leistner, Voltage-controlled ON switching and manipulation of magnetization via the redox transformation of β -FeOOH nanoplatelets, J. Phys. D Appl. Phys. **53**, 084001 (2020).

[25] A. Quintana, A. A. Firme, C. J. Jensen, D. Zheng, C. Liu, X. Zhang, and K. Liu, Hydroxide-based magneto-ionics: Electric-field control of a reversible paramagnetic-to-ferromagnetic switch in α-$Co(OH)_2$ films, J. Mater. Chem. C **10**, 17145 (2022).

[26] A. J. Tan, M. Huang, C. O. Avci, F. Büttner, M. Mann, W. Hu, C. Mazzoli, S. Wilkins, H. L. Tuller, and G. S. D. Beach, Magneto-ionic control of magnetism using a solid-state proton pump, Nat. Mater. **18**, 35 (2019).

[27] F. Maroun, F. Reikowski, N. Di, T. Wiegmann, J. Stettner, O. M. Magnussen, and P. Allongue, Potential dependence of the structure and magnetism of electrodeposited Pd/Co/Au(111) layers, J. Electroanal. Chem. **819**, 322 (2018).

[28] A. Quintana, E. Menéndez, M. O. Liedke, M. Butterling, A. Wagner, V. Sireus, P. Torruella, S. Estradé, F. Peiró, J. Dendooven *et al.*, Voltage-controlled on–off ferromagnetism at room temperature in a single metal oxide film, ACS Nano **12**, 10291 (2018).

[29] J. Zehner, I. Soldatov, S. Schneider, R. Heller, N. B. Khojasteh, S. Schiemenz, S. Fähler, K. Nielsch, R. Schäfer, and K. Leistner, Voltage-controlled deblocking of magnetization reversal in thin films by tunable domain wall interactions and pinning sites, Adv. Electron. Mater. **6**, 2000406 (2020).

[30] D. A. Gilbert, A. J. Grutter, E. Aarenholz, K. Liu, B. J. Kirby, J. A. Borchers, and B. B. Maranville, Structural and magnetic depth profiles of magneto-ionic heterostructures beyond the interface limit, Nat. Commun. **7**, 12264 (2016).

[31] N. N. Di, J. Kubal, Z. Zeng, J. Greeley, F. Maroun, and P. Allongue, Influence of controlled surface oxidation on the magnetic anisotropy of Co ultrathin films, Appl. Phys. Lett. **106**, 122405 (2015).

[32] C. Navarro-Senent, J. Fornell, E. Isarain-Chávez, A. Quintana, E. Menéndez, M. Foerster, L. Aballe, E. Weschke, J. Nogués, E. Pellicer, and J. Sort, Large magnetoelectric effects in electrodeposited nanoporous microdisks driven by effective surface charging and magneto-ionics, ACS Appl. Mater. Interfaces **10**, 44897 (2018).

[33] N. Tournerie, A. P. Engelhardt, F. Maroun, and P. Allongue, Influence of the surface chemistry on the electric-field control of the magnetization of ultrathin films, Phys. Rev. B **86**, 104434 (2012).

[34] A. E. Kossak, D. Wolf, and G. S. D. Beach, Magneto-ionic enhancement and control of perpendicular magnetic anisotropy, Appl. Phys. Lett. **121**, 222402 (2022).

[35] M. Bischoff, R. Ehrler, F. Engelhardt, O. Hellwig, K. Leistner, and M. Gößler, Magneto-ionic control of coercivity and domain-wall velocity in Co/Pd multilayers by electrochemical hydrogen loading, Adv. Funct. Mater. **34**, 2405323 (2024).

[36] M. Gößler, M. Albu, G. Klinser, E. Steyskal, H. Krenn, and R. Würschum, Magneto-ionic switching of superparamagnetism, Small **15**, 1904523 (2019).

[37] X. Ye, X. Zhu, H. Yang, J. Duan, S. Gao, C. Sun, X. Liu and R.-W. Li, Selective dual-ion modulation in solid-state magnetoelectric heterojunctions for in-memory encryption, Small **19**, 2206824 (2023).

[38] H.-B. Li, N. Lu, Q. Zhang, Y. Wang, D. Feng, T. Chen, S. Yang, Z. Duan, Z. Li, Y. Shi *et al.*, Electric-field control of ferromagnetism through oxygen ion gating, Nat. Commun. **8**, 2156 (2017).

[39] H. J. Bauer and E. Schmidbauer, Über den Einfluss elektrolytischer Wasserstoffbeladung auf die Magnetisierung von Nickel, Z. Physik **164**, 367 (1961).

[40] J.-Z. Yu, Q. Sun, Q. Wang. and Y. Kawazoe, Effect of hydrogen on the magnetism and its solubility in ferromagnetic nickel, Mater. Trans. JIM **40**, 1244 (1999).

[41] A. León, E. A. Velásquez, J. Mazo-Zuluaga, J. Mejía-López, J. M. Florez. and P. Vargas, Magnetic effects of interstitial hydrogen in nickel, J. Magn. Magn. Mater. **421**, 7 (2017).

[42] V. Vij, S. Sultan, A. M. Harzandi, A. Meena, J. N. Tiwari, W.-G. Lee, T. Yoon and K. S. Kim, Nickel-based electrocatalysts for energy-related applications: Oxygen reduction, oxygen evolution, and hydrogen evolution reactions, ACS Catal. **7**, 7196 (2017).

[43] T. Shinagawa and K. Takanabe, Towards versatile and sustainable hydrogen production through electrocatalytic water splitting: Electrolyte engineering, Chem. Sus. Chem. **10**, 1318 (2017).

[44] J. Tan and J. Liu, Electrolyte engineering toward high-voltage aqueous energy storage devices, Energy Environ. Mater. **4**, 302 (2021).

[45] S. Martins, Z. Ma, X. Solans-Monfort, M. Sodupe, L. Rodriguez-Santiago, E. Menendez, E. Pellicer and J. Sort, Enhancing magneto-ionic effects in cobalt oxide films by electrolyte engineering, Nanoscale Horiz. **8**, 118 (2023).

[46] J. Zehner, O. Vaerst, I. Soldatov, K. Nielsch, R. Schafer and K. Leistner, Robust magneto-ionic effect in Fe/FeO_x thin films in electrolytes with different cations, IEEE Trans. Magn. **58**, 6000108 (2022).

[47] A. Mituya, K. Sekine and G. Toda, Determination of diffusion coefficient of hydrogen through nickel foil, J. Res. Instit. Catalys. Hokkaido Univ. **15**, 21 (1967).

[48] G. A. Di Bari, Electrodeposition of Nickel, in *Modern Electroplating*, edited by M. Schlesinger and M. Paunovic, (Wiley, Hoboken, NJ, 2010), pp. 79–114.

[49] See Supplemental Material at http://link.aps.org/supplemental/10.1103/29bv-d9j4 for Auger electron spectroscopy depth profile (S1), Scheme of *in situ* SQUID and MOKE cells (S2), Magnetic hysteresis (S3), first *in situ* SQUID cycle for KOH (S4), *in situ* Raman spectra (S5), DFT calculations (S6), *in situ* SQUID for KOH with thiourea (S7), *in situ* MOKE for 1000 Red-Ox cycles (S8), Calculation of the influence of adsorbed H (Note S1), Estimation of Ni layer thickness using the moment change (Note S2), which also includes Refs. [50–55].

[50] B. P. Payne, A. P. Grosvenor, M. C. Biesinger, B. A. Kobe and N. S. McIntyre, Structure and growth of oxides on polycrystalline nickel surfaces, Surf. Interf. Anal. **39**, 582 (2007).

[51] S. Ghosh, B. Dasgupta, S. Kalra, M. L. P. Ashton, R. Yang, C. J. Kueppers, S. Gok, E. G. Alonso, J. Schmidt, K. Laun, I. Zebger *et al.*, Evolution of carbonate-intercalated γ-NiOOH from a molecularly derived nickel sulfide (pre)catalyst for efficient water and selective organic oxidation, Small **19**, 2206679 (2023).

[52] Z. Qiu, C.-W. Tai, G. A. Niklasson, and T. Edvinsson, Direct observation of active catalyst surface phases and the effect of dynamic self-optimization in NiFe-layered double hydroxides for alkaline water splitting, Energy Environ. Sci. **12**, 572 (2019).

[53] L. E. Kalichkina, P. K. Krivolapenko, and V. P. Tuguldurova, Quantitative Raman spectroscopy of urea and thiourea in the reaction mixtures of allantoin and 4,5-dihydroxyimidazolidine-2-Tione formation, J. Raman Spectrosc. **55**, 1165 (2024).

[54] K. Christmann, O. Schober, G. Ertl, and M. Neumann, Adsorption of hydrogen on nickel single crystal surfaces, J. Chem. Phys. **60**, 4528 (1974).

[55] M. Oshitani, T. Takayama, K. Takashima, and S. Tsuji, A study on the swelling of a sintered nickel hydroxide electrode, J. Appl. Electrochem. **16**, 403 (1986).

[56] D. S. Hall, C. Bock, and B. R. MacDougall, The electrochemistry of metallic nickel: Oxides, hydroxides, hydrides and alkaline hydrogen evolution, J. Electrochem. Soc. **160**, F235 (2013).

[57] S. Topolovec, H. Krenn, and R. Würschum, Electrochemical cell for *in situ* electrodeposition of magnetic thin films in a superconducting quantum interference device magnetometer, Rev. Sci. Instr. **86**, 063903 (2015).

[58] I. V. Soldatov and R. Schäfer, Selective sensitivity in Kerr microscopy, Rev. Sci. Instr. **88**, 073701 (2017).

[59] I. V. Soldatov and R. Schäfer, Advanced MOKE magnetometry in wide-field Kerr-microscopy, J. Appl. Phys. **122**, 153906 (2017).

[60] K. Koepernik and H. Eschrig, Full-potential nonorthogonal local-orbital minimum-basis band-structure scheme, Phys. Rev. B **59**, 1743 (1999).

[61] https://www.fplo.de/.

[62] J. P. Perdew, K. Burke, and M. Ernzerhof, Generalized gradient approximation made simple, Phys. Rev. Lett. **77**, 3865 (1996).

[63] S. L. Medway, C. A. Lucas, A. Kowal, R. J. Nichols, and D. Johnson, *In situ* studies of the oxidation of nickel electrodes in alkaline solution, J. Electroanal. Chem. **587**, 172 (2006).

[64] J. Proost and A. Delvaux, In-situ monitoring of hydrogen absorption into Ni thin film electrodes during alkaline water electrolysis, Electrochim. Acta **322**, 134752 (2019).

[65] D. S. Hall, D. J. Lockwood, S. Poirier, C. Bock, and B. R. MacDougall, Applications of *in situ* Raman spectroscopy for identifying nickel hydroxide materials and surface layers during chemical aging, ACS Appl. Mater. Interf. **6**, 3141 (2014).

[66] D. S. Hall, D. J. Lockwood, C. Bock, and B. R. MacDougall, Nickel hydroxides and related materials: A review of their structures, synthesis and properties, Proc. R. Soc. A. **471**, 20140792 (2015).

[67] R. Kostecki and F. McLarnon, Electrochemical and *in situ* raman spectroscopic characterization of nickel hydroxide electrodes: I. Pure nickel hydroxide, J. Electrochem. Soc. **144**, 485 (1997).

[68] J. D. Rall, M. S. Seehra, N. Shah, and G. P. Huffman, Comparison of the nature of magnetism in and β-$Ni(OH)_2$, J. Appl. Phys. **107**, 09B511 (2010).

[69] P. W. Selwood, Magnetic saturation results for H_2/Ni, H_2/Ni–Cu, H_2/Co, and H_2/Fe, in *Chemisorption and Magnetization* (Elsevier, Amsterdam, 1975), p. 55–65.

[70] E. B. Ferreira and G. Jerkiewicz, On the electrochemical reduction of β-$Ni(OH)_2$ to metallic nickel, Electrocatal. **12**, 199 (2021).

[71] K. Duschek, D. Pohl, S. Fähler, K. Nielsch, and K. Leistner, Research Update: Magnetoionic control of magnetization and anisotropy in layered oxide/metal heterostructures, APL Mater. **4**, 032301 (2016).

[72] A. Ramesh, M. R. Govindaraju, D. C. Jiles, S. B. Biner, and J. M. Roderick, Hydrogen charging in nickel and iron and its effect on their magnetic properties, J. Appl. Phys. **79**, 5453 (1996).

[73] J. K. Blum and W. Göpel, Influence of hydrogen chemisorption on the magnetism of thin nickel films, Thin. Solid. Films **42**, 7 (1977).

[74] L. Mirkova, G. Maurin, M. Monev, and C. Tsvetkova, Hydrogen coevolution and permeation in nickel electroplating, J. Appl. Electrochem. **33**, 93 (2003).

[75] T. M. Harris and M. Latanision, Grain boundary diffusion of hydrogen in nickel, Metall. Trans. A **22**, 351 (1991).

[76] A. Y. Faid, A. O. Barnett, F. Seland, and S. Sunde, Ni/NiO nanosheets for alkaline hydrogen evolution reaction: *In situ* electrochemical-Raman study, Electrochim. Acta **361**, 137040 (2020).

[77] D. S. Hall, D. J. Lockwood, S. Poirier, C. Bock, and B. R. MacDougall, Raman and infrared spectroscopy of α and β phases of thin nickel hydroxide films electrochemically formed on nickel, J. Phys. Chem. A **116**, 6771 (2012).

[78] M. W. Louie and A. T. Bell, An investigation of thin-film Ni–Fe oxide catalysts for the electrochemical evolution of oxygen, J. Am. Chem. Soc. **135**, 12329 (2013).

[79] M. Jayalakshmi, P. Radhika, K. P. Raja, and M. M. Rao, Solvent and thiourea adsorption/intercalation effects on the solid-state electrochemistry of α-phase nickel hydroxide nanoparticles, J. Solid State Electrochem. **11**, 165 (2006).

[80] B. Baranowski and Z. Szklarska-Smialowska, A galvanostatic and potentiostatic study of the nickel-hydrogen system, Electrochim. Acta **9**, 1497 (1964).

[81] Y. Oren, E. Elish, A. Tamir, and Z. Gavra, A dilatometric study of nickel wire electrode electrochemically charged by hydrogen, J. Alloys Comp. **235**, 30 (1996).

[82] W. Visscher and E. Barendrecht, Absorption of hydrogen in reduced nickel oxide, J. Appl. Electrochem. **10**, 269 (1980).

[83] L. Wang, C. Lin, D. Huang, J. Chen, L. Jiang, M. Wang, L. Chi, L. Shi, and J. Jin, Optimizing the volmer step by single-layer nickel hydroxide nanosheets in hydrogen evolution reaction of platinum, ACS Catal. **5**, 3801 (2015).

[84] W. Lai, L. Ge, H. Li, Y. Deng, B. Xu, B. Ouyang, and E. Kan, *In situ* Raman spectroscopic study towards the growth and excellent HER catalysis of Ni/$Ni(OH)_2$ heterostructure, Int. J. Hydrogen Energy **46**, 26861 (2021).

[85] S. Xue, Y. Liang, S. Hou, Y. Zhang, and H. Jiang, Alpha-nickel hydroxide coating of metallic nickel for enhanced

alkaline hydrogen evolution, Chem. Sus. Chem **15**, e202201072 (2022).

[86] E. Protopopoff and P. Marcus, Surface effects on hydrogen entry into metals, in *Corrosion Mechanisms in Theory and Practice*, edited by P. Marcus, (CRC Press, Boca Raton, FL, 2002), Vol. 17, p. 53–96.

[87] M. Guan, L. Wang, S. Zhao, B. Peng, W. Su, Z. He, G. Dong, T. Min, J. Ma, Z. Hu *et al.*, Ionic modulation of interfacial magnetism in light metal/ferromagnetic insulator layered nanostructures, Adv. Funct. Mater. **29**, 1805592 (2019).

[88] M. Kutuzau, M. Gößler, S. Topolovec, S. Schiemenz, D. Wolf, M. Richter, K. Nielsch, and K. Leistner, Dataset for the manuscript "Additive-enhanced hydrogen- and hydroxide-based magneto-ionic control in Ni films," Zenodo (2025), doi:10.5281/zenodo.17417586.